Applied Catalysis B: Environmental 180 (2016) 106–112

Contents lists available at ScienceDirect

Applied Catalysis B: Environmental

journal homepage: www.elsevier.com/locate/apcatb

Silica nanocrystal/graphene composite with improved photoelectric and photocatalytic performance

Lingang Yang, Lingzhi Wang*, Mingyang Xing, Juying Lei, Jinlong Zhang*

Key Laboratory for Advanced Materials and Institute of Fine Chemicals, East China University of Science and Technology, 130 Meilong Road, Shanghai 200237, PR China

ARTICLE INFO

Article history:
Received 4 May 2015
Received in revised form 9 June 2015
Accepted 13 June 2015
Available online 19 June 2015

Keywords:
Vinyltriethoxysilane
Silica nanocrystal
rGO
Photoelectric
Photocatalysis

ABSTRACT

A modified Stöber process using vinyltriethoxysilane as the precursor and in the presence of graphene oxide unprecedentedly leads to the exclusive growth of monodispersed silica nanocrystals (SiO_2 NCs) (ca. 3–4 nm) at room-temperature on single-layer graphene sheet with a high deposition density (ca. $10^{16}/m^2$), where graphene oxide is simultaneously reduced by ammonia. Well-resolved lattice fringes with the spacing of 0.19 nm demonstrate the excellent crystallinity of SiO_2 NC, which has an absorption band in the range of 200–400 nm. The anchoring of vinyl-silanols on graphene oxide through Si—O—C oxo-bridging and the π–π interaction between double bonds of vinyl-silanols and graphene oxide co-direct the orderly growth of SiO_2 NC nuclei on graphene. Compared with isolate and physically mixed SiO_2 and graphene, the composite has decreased impedance and 4.5 times improved photocurrent, which also shows extraordinarily high photocatalytic activity toward the degradation of organic pollutant.

1. Introduction

Reduced graphene oxide (rGO) with high carrier mobility and large specific surface area has drawn tremendous attention from the fields of energy and environment [1–6]. Recent years have witnessed the prosperous development of graphene-based functional composites benefited from the scalable and reliable production of rGO [7–9]. Particularly, semiconductor/rGO composite has shown great potential applications in solar cell, lithium ion battery and photocatalysis, with significantly improved electric or photoelectric performance benefited from the coupling interaction between rGO and semiconductor [10–13]. To achieve a strong coupling effect, the contact area and combination force need to be maximized, which requires a high deposition density of semiconductor and an intimate contact between rGO and semiconductor [14–16].

Generally, semiconductor/rGO can be prepared from the post-loading or in-situ growth of metal oxide/sulfide and quantum dots on granphene sheet [17–22]. In-situ growth of semiconductor on rGO has proven to be more effective on improving the combination force than the post-loading route [15]. However, controlling on the selective growth of semiconductor on rGO as well as the particle size, uniform distribution and the deposition density of loaded semiconductor is important for the application performance but still remains a great challenge. Compared with rGO, GO with abundant epoxy and carbonyl groups is more efficient on improving the selective growth rate of semiconductor mainly by utilizing the interactions between metal ions and oxygen-containing groups of GO including electrostatic attraction and complexation [23]. The current routes unavoidably require high-temperature calcination or hydrothermal process to crystallize metal oxide and reduce GO [24,25], which however easily leads to the stacking of rGO and the local aggregation of semiconductor particles. Therefore, great efforts on exploring novel synthetic strategy still need to be paid to seek the possibility on solving the current development bottleneck [26].

Here, we present the first room-temperature synthesis of silica nanocrystal on rGO (SiO_2 NC/rGO) from a modified Stöber process with vinyltriethoxysilane(VTES) as the precursor and GO as the additive through a finely controlled nucleation and growth behavior of vinyl-silanols on GO, which is simultaneously ammonia-reduced to rGO after the reaction. Monodispersed SiO_2 NCs (ca. 3–4 nm) with excellent crystallinity are exclusively grown on rGO with a high deposition density (ca. $10^{16}/m^2$). Amorpous SiO_2 is formed in the absence of GO. In comparison with isolate and physically mixed SiO_2 and graphene, the composite possesses decreased impedance and improved photoelectric performance under irradiation, which also shows high activity toward the photocatalytic degradation of rhodamine B and 2, 4-dichlorophenol.

* Corresponding authors. Fax: +86 21 64252062.
E-mail addresses: wlz@ecust.edu.cn (L. Wang), jlzhang@ecust.edu.cn (J. Zhang).

http://dx.doi.org/10.1016/j.apcatb.2015.06.026
0926-3373/

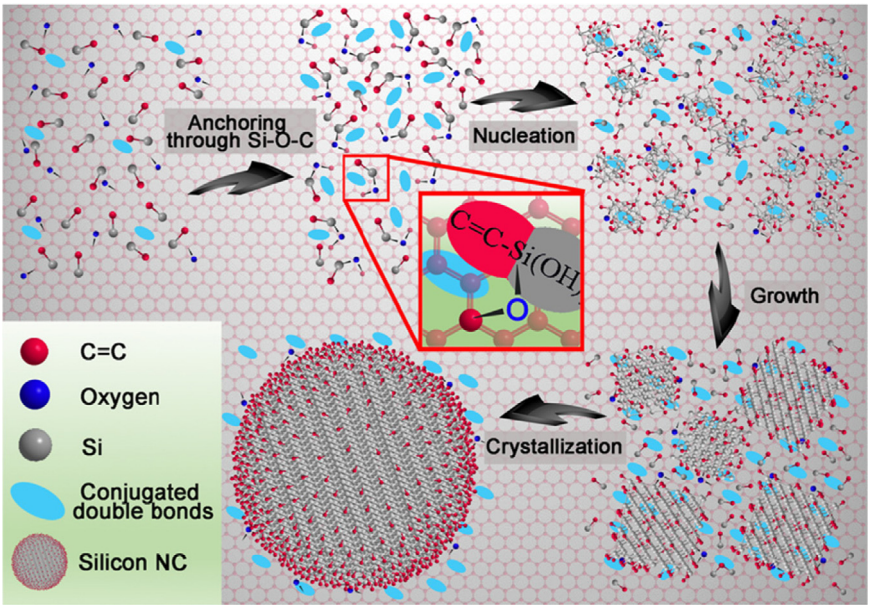

Scheme 1. Scheme for the formation mechanism of SiO_2 NC/rGO.

2. Experimental

2.1. Materials

All chemicals, including Vinyltriethoxysilane (VTES) (CP), $NH_3{\cdot}H_2O$ (AR), EtOH (AR), H_2SO_4 (AR), $NaNO_3$ (AR), $KMnO_4$ (AR) and H_2O_2 (AR) were used as received without any further purification. 2, 4-dichlorophenol (2, 4-DCP), Rhodamine B (RhB) and Graphite was purchased from Sigma–Aldrich, and ultrapure water was used for all experiments.

2.2. Preparation and characterization

Graphite oxide (GO) was synthesized from natural graphite using a modified Hummers methods [18,27,35,36]. In a typical process, a certain amount of VTES and $NH_3{\cdot}H_2O$ were dispersed into solution containing 20 mL GO (1 mg/mL), 10 mL EtOH and 50 mL H_2O under magnetic stirring. The SiO_2 NC/rGO aqueous solution could be obtained after keeping stirred at R.T. for 24 h. The amorphous SiO_2 was synthesized in the absence of GO. The composite obtained by physically mixing rGO and amorphous SiO_2 synthesized in the absence of GO was denoted as SiO_2–rGO. In experiment, the volume concentrations of ammonia (0.55%, 0.83%, 1.10%, 1.38%, 1.65%, 2.20%) and VTES (0.03%, 0.06%, 0.12%, 0.24%) were adjusted to investigate the influence of experimental condition to the formation of SiO_2 NC/rGO hybrid.

X-ray diffraction (XRD) patterns of all samples were collected in the range 10–80° (2θ) using a Rigaku D/max 2550 diffractometer (Cu Kα radiation, λ = 1.5406 Å), operated at 40 kV and 100 mA. A NanoScope IIIa MultiMode atomic force microscope (AFM) was used to probe the thickness of GO sheet. The transmission electron microscopy (TEM) was conducted on a JEOL JEM-2100EX electron microscope, operated at an accelerating voltage of 200 KV. The instrument employed for XPS studies was a PerkinElmer PHI 5000C ESCA system with $Al_{K\alpha}$ radiation operated at 250 W. The shift of the binding energy due to relative surface charging was corrected using the C1s level at 284.6 eV as an internal standard. The concentration of RhB was measured using a UV–vis spectrophotometer (Shimadzu, UV-2450). The concentration of 2, 4-DCP was determined by Shimadzu LC-20A high performance liquid chromatography (HPLC). Raman measurements were performed at room temperature using a Via + Reflex Raman spectrometer with the excitation wavelength of 514 nm. The electrochemical experiments included electro-chemical impedance spectra (EIS) and photocurrents measurements were carried out on an electrochemical analyzer (CHI 660 D electrochemical station, CHI Instruments Inc.) at room temperature.

2.3. Photocatalytic activities

The photocatalytic activity of each sample was evaluated in terms of the degradation of Rhodamine B (RhB, 10 mg/L). The SiO_2 NC/rGO hybrid was added into a 100 mL quartz photo-reactor containing 50 mL of RhB solution and 12.5 mg of photocatalyst. A 300 W Xe lamp was used as the light source. All of the degradation was carried out after a dark adsorption process for 3 h to ensure adsorption equilibrium. At the given time intervals, the analytical samples were taken from the mixture and immediately centrifuged before filtration through a 0.22 μm millipore filter to remove the photocatalysts. The filtrates were analyzed by recording variations in the absorption in UV–vis spectra of RhB using a Cary 100 ultraviolet visible spectrometer. The photocatalytic activity was also evaluated by using 2, 4-dichlorophenol as the pollutant model (2, 4-DCP, 10 mg/L). The degradation process of 2, 4-DCP was similar with the degradation of RhB except that the concentration of 2, 4-DCP was determined by high performance liquid chromatography (HPLC).

3. Results and discussion

3.1. Preparation and characteriazation of catalysts

Ultrathin sheet with SiO_2 NCs exclusively deposited on it is first revealed by the transmission electron microscopy (TEM) image of SiO_2 NC/rGO composite prepared from 0.12% volume concentration of VTES (Fig. 1A). The enlarged image shows that SiO_2 NCs are monodispersed with high deposition density (ca. $10^{16}/m^2$) (Fig. 1B and C) and have uniform size distribution between 3 and 4 nm (Inset, Fig. 1B). The atom percentage of Si revealed by EDX spectrum

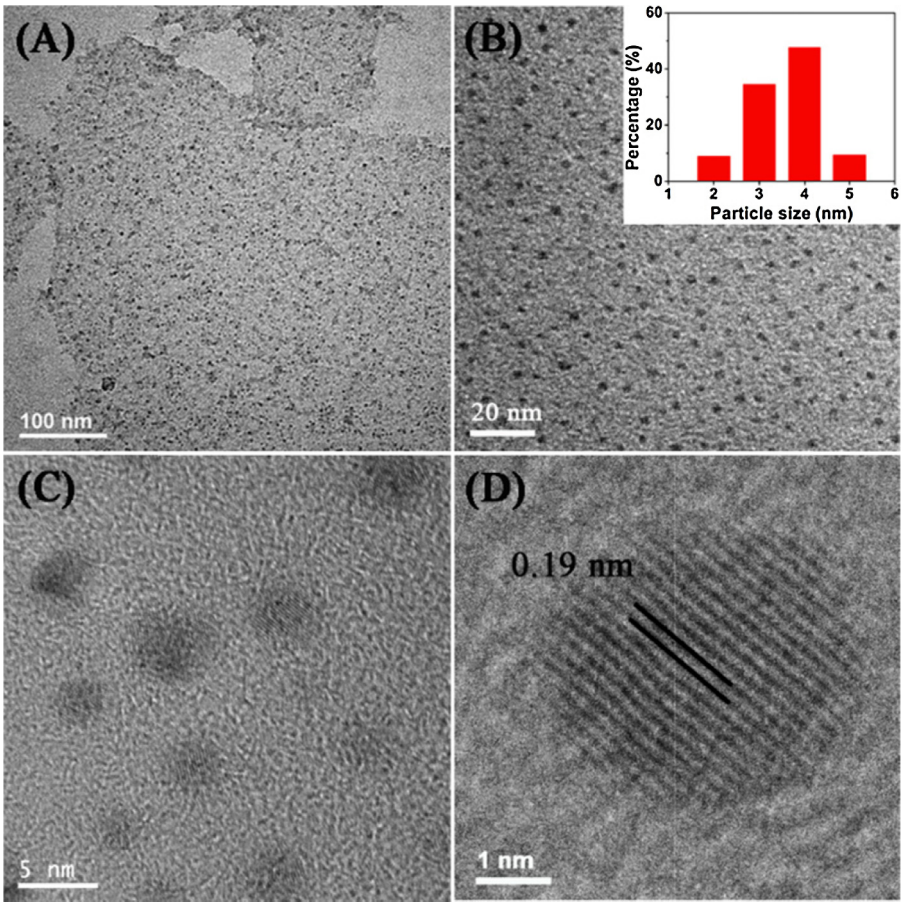

Fig. 1. (A–C) TEM and (D) HRTEM images of SiO_2 NC/rGO composite.

is about 20% (Fig. S1), further proving the high loading efficiency of SiO_2 NCs. Well-resolved lattice fringes with the spacing of 0.19 nm demonstrate the excellent crystallinity of SiO_2 NC as evidenced by the high resolution TEM (HRTEM) microscopy (Fig. 1D). In comparison, the absence of GO in the sol–gel process of VTES leads to the formation of amorphous and severely aggregated SiO_2 (Fig. S2), which can't be further dispersed on rGO through physical mixing (Fig. S3). The deposition density of SiO_2 NCs can be further increased by increasing the volume concentration of VTES. However, a concentration over 0.24% produces submicrometer-sized amorphous SiO_2 separated from graphene (Fig. S4), which should be attributed to an explosive nucleation of free VTES molecules when the loading capacity of GO is over-saturated. Even in this case, loaded SiO_2 NC still retain the monodispersity, indicating a strong capability of the carrier on controlling the nucleation and growth behavior of SiO_2 NC.

It is noted that the gel color changes from yellowish–brown to black after the reaction (Fig. 2A), which is attributed to the reduction of GO to rGO as verified by the shift of G band from 1597 to 1587 cm^{-1} in the Raman spectra (Fig. 2B) [24]. Si 2p X-ray photoelectron spectroscopy (XPS) spectrum of the composite indicates the existence of Si—O—C bond (101.9 eV) (Fig. 2C) [28,29,31]. The C 1s spectra imply the epoxy (286.8 eV) groups of GO are significantly decreased after the sol–gel process, verifying the reduction of GO (Fig. 2D and E). Moreover, new peaks appear at 286.2 eV and 290.2 eV, ascribing to the formation of Si—O—C and Si—O—C=O, respectively [30,31]. To understand the reason for the GO reduction in a sol–gel system, control experiments were carried out in the absence of VTES or ammonia. Results from XPS spectra indicate the reduction of GO without VTES (Fig. 2F), while the absence of ammonia fails to reduce GO, revealing the presence of ammonia is responsible for the GO reduction (Fig. S5). This result is accordant with the previous report about the reduction of GO by NaOH [32]. Therefore, the sol–gel process of VTES in the presence of GO simultaneously leads to the formation of SiO_2 NCs and rGO.

Further characterization by atomic force microscopy (AFM) indicates the thickness of SiO_2 NC/rGO is about 1.0 nm (Fig. 3A), a little higher than that of single-layer rGO [33], indicating rGO is stacking-free during the reduction process and SiO_2 NC is flatly grown on rGO. The aggregation-free rGO sheet should be benefited from the mild reaction process. The wide-angle X-ray diffraction (WAXRD) pattern of the composite only shows a broad peak attributed to rGO (Fig. 3B). The lack of diffraction peak belonging to crystallized silicon should be due to its tiny particle size. GO shows an absorption band below 400 nm with a maximum absorbance at 230 nm (Fig. 3C). The absorption range is extended to almost the whole visible light range and the absorbance of the original band is also increased after the ammonia treatment, indicative of the formation of rGO with improved conjugation degree. The absorbance in the UV range is SiO_2 NC/rGO using the absorption of rGO obtained in the absence of VTES as the reference indicates a wide absorption band composed of two peaks centered at 250 nm and 300 nm (Fig. 3D), which should be attributed to the absorbance of SiO_2 NCs. No photoluminescence is observed from the composite (Fig. S6). As the end group of VTES, vinyl should be distributed on the surface of SiO_2 NC and overlapped with the double bonds of graphene, leading to a large π-conjugated system. The negligible photoluminescence of SiO_2 NCs on rGO suggests the excited electron does not jump back to the ground state in the form of light-emission [34], which

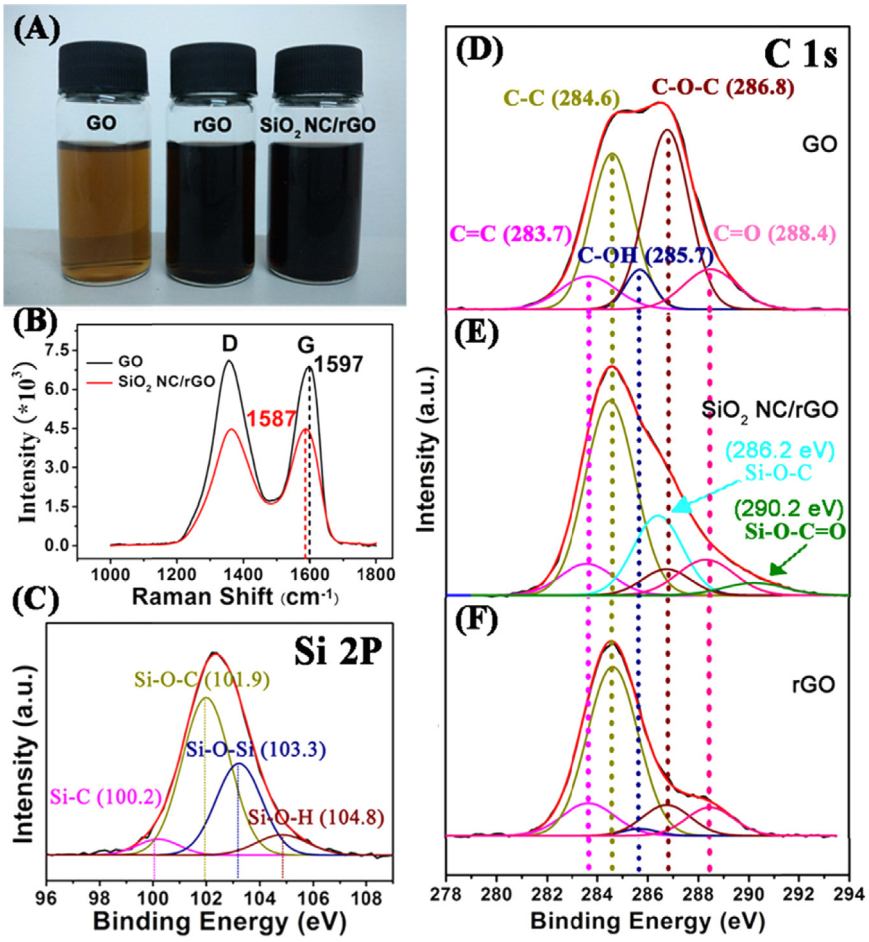

Fig. 2. (A) Photographs of GO, rGO and SiO_2 NC/rGO, (B) Raman spectra of GO and SiO_2 NC/rGO, (C) Si 2p XPS spectrum of SiO_2 NC/rGO and (D) C 1s XPS spectra of GO, SiO_2 NC/rGO and rGO.

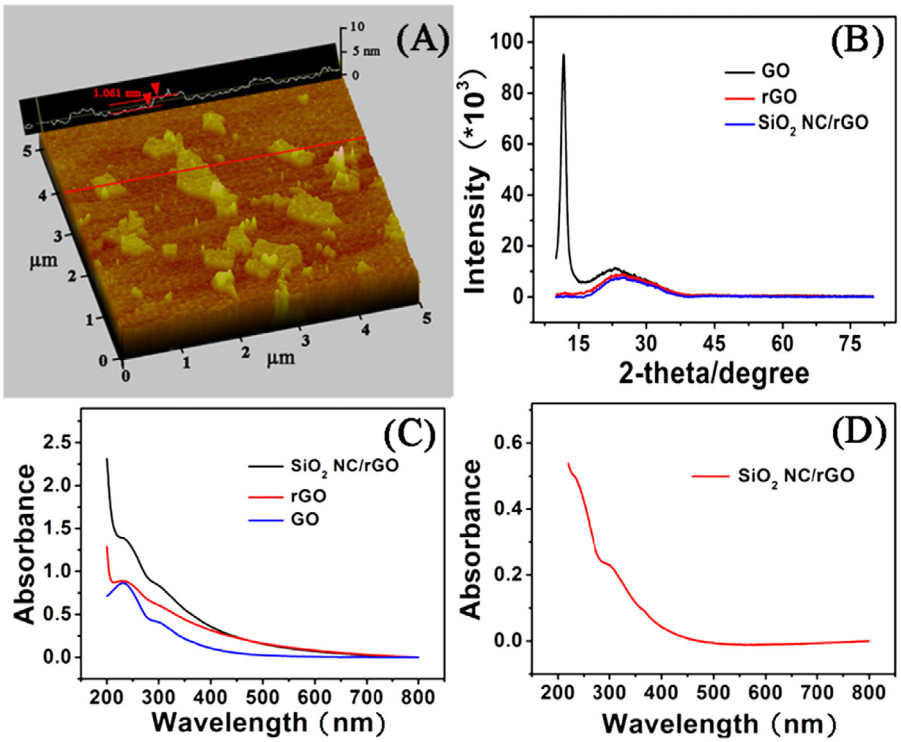

Fig. 3. (A) AFM image and (B) WAXRD pattern of SiO_2 NC/rGO, (C) UV–vis absorption spectra of GO, rGO and SiO_2 NC/rGO, (D) Differential UV–vis absorption spectrum of SiO_2 NC/rGO using the absorption of rGO obtained in the absence of VTES as the reference.

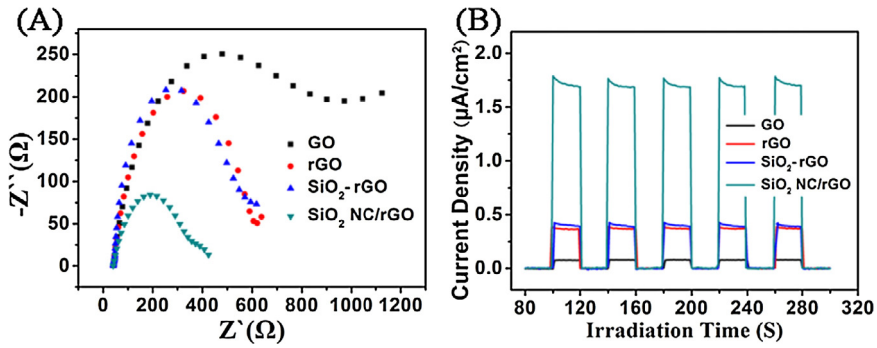

Fig. 4. (A) Electrochemical impedance spectra of GO, rGO, SiO_2–rGO and SiO_2 NC/rGO, (B) Photocurrent of GO, rGO, SiO_2–rGO and SiO_2 NC/rGO under the irradiation of simulated solar light.

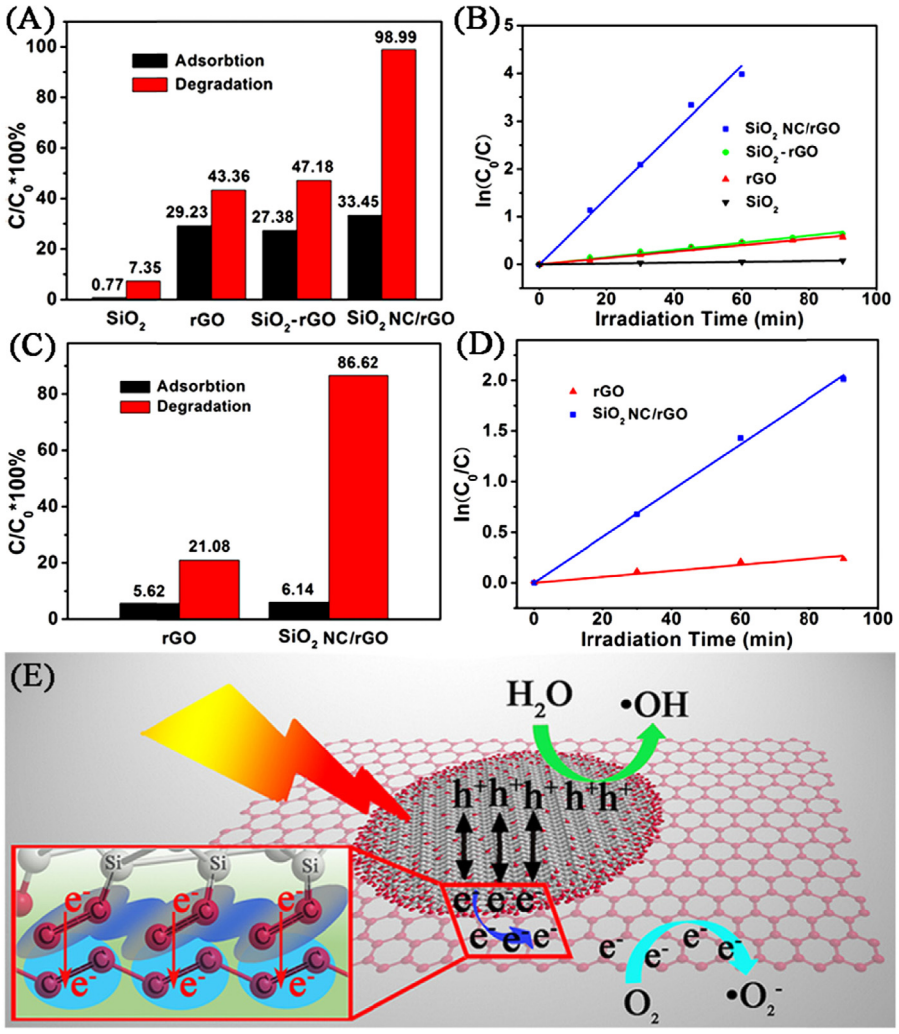

Fig. 5. (A) Adsorption and photocatalytic elimination percentages and (B) first-order kinetic degradation curves of RhB on SiO_2, rGO, SiO_2–rGO and SiO_2 NC/rGO, (C) Adsorption and photocatalytic elimination percentages and (D) First-order kinetic curves for the degradation of 2, 4-DCP on rGO and SiO_2 NC/rGO, (E) Scheme for electron transfer from SiO_2 NCs to rGO under light irradiation.

actually immediately transfers to rGO due to the strongly coupling of π-conjugated system between SiO_2 NCs and rGO carrier.

3.2. Formation mechanism of SiO_2 NC/rGO

To accurately understand the formation mechanism of SiO_2 NCs on rGO at room temperature, the influence of synthetic parameters including ammonia concentration and reaction temperature have been further investigated. The SiO_2 NCs deposition density on rGO increases with the increasing volume concentration of ammonia. However, amorphous and aggregated SiO_2 is formed when the ammonia concentration exceeds to 1.65% (Fig. S7). Increasing the reaction temperature from 0 to 30 °C leads to the increasing deposition density of SiO_2 NCs, but an over high temperature of 45 °C results in a poor deposition efficiency (Fig. S8). Raman spectra indicate the intensity ratio of D/G increases more quickly at higher

ammonia concentration and reaction temperature (Fig. S9), suggesting the reduction extent and kinetics of GO are accelerated in these conditions. Moreover, a pure EtOH system fails to form SiO_2 NC and reduction of GO, while a pure water system cause the coating-like growth of amorphous SiO_2 on rGO (Fig. S10), which indicate the presence of appropriate amount of H_2O in the reaction system is necessary to the formation of SiO_2 NCs on rGO. Based on the above results, a controlled nucleation and growth behavior of SiO_2 NCs on graphene oxide is revealed as follows (Scheme 1). In the Stöber system using VTES as the precursor, the hydrolytic speed of VTES molecule is extremely slow due to its low volume concentration (<0.24%) and the existence of vinyl group. The presence of vinyl groups further induces the selective deposition of vinyl-silanols hydrolyzed from VTES on GO in the EtOH/H_2O solution due to their similar chemical composition. After the deposition, vinyl-silanols are first anchored on GO through Si—O—C oxo-bridging and them slowly form into SiO_2 NC nuclei. Finally, the π–π stacking force between double-bonds of SiO_2 NC nuclei and GO, and the increased π-conjugation degree of rGO further direct the growth of SiO_2 NC nuclei in an orderly way. The ammonia-reduction process of GO should be slow enough to be synchronic with the hydrolysis speed of VTES and the subsequent growth of SiO_2 NC nuclei, which requires a low ammonia concentration or reaction temperature.

3.3. Photoelectric and photocatalytic performance

Result from the electrochemical impedance analysis indicates the impedance of rGO is decreased after the deposition of SiO_2 NCs (Fig. 4A). The surface of SiO_2 NCs is covered with high-density vinyl groups overlapped with each other, which should lead to the increase of π-conjugation degree of the composite compared with pure rGO due to the intimate contact between SiO_2 NCs and rGO. The composite with enhanced π-conjugation system thus presents better ability of electron mobility. Under the irradiation of simulated solar light, the photocurrent intensity of SiO_2 NCs/rGO is 4.5-fold improved compared with those of rGO and a physical mixture of SiO_2 and rGO (Fig. 4B). The improved photocurrent should be attributed to the efficient electron charging from SiO_2 NCs to rGO.

In consideration of the semiconducting characteristic of SiO_2 NCs on rGO, the composite was further applied to the degradation of rhodamine B (Rh B). All of the degradation was carried out after a dark adsorption process for 3 h to ensure adsorption equilibrium. A complete degradation of 10 mg/L RhB is achieved within 45 min in the presence of 0.25 g/L SiO_2 NC/rGO (Fig. 5A, Fig. S11). In comparison, only 15% RhB is eliminated by rGO and the physically mixed rGO and amorphous SiO_2 synthesized in the absence of GO (SiO_2–rGO). Negligible degradation is observed from the isolate amorphous SiO_2. A high kinetic parameter of 0.070 min^{-1} is obtained by fitting the degradation curve with first-order kinetic equation (Fig. 5B). According to the result from the dark adsorption experiment (Fig. 5A), the high efficiency is partly attributed to the improved dark-adsorption ability of rGO. Amorphous SiO_2 shows negligible adsorption to pollutant (0.77%). All rGO-involved samples show about 30% capture of RhB after the adsorption equilibrium. To eliminate the effect of dye self-sensitization on the photocatalytic activity, colorless 2, 4-dichlorophenol (2, 4-DCP) was further adopted as the pollutant target, a higher degradation kinetic parameter of SiO_2 NC/rGO (0.023 min^{-1}) is obtained compared with that on rGO (0.003 min^{-1}) (Fig. 5C and D), indicating the superior photocatalytic performance of our composite. The high photocatalytic efficiency should be attributed to the non-blocked electron transport from semiconducting SiO_2 NCs to reduced graphene due to their intimate contact and the formation of strongly coupled π-conjugation system (Fig. 5E).

4. Conclusions

In conclusion, SiO_2 NC/rGO with monodispersed SiO_2 NCs exclusively and homogenously distributed on rGO is synthesized at room temperature from a modified Stöber process using vinyltriethoxysilane as the precursor and in the presence of GO, where GO is simultaneously reduced to rGO by ammonia. The chemical similarity between vinyl-silanol and GO and their synchronized reaction process are necessary prerequisites to achieve the orderly growth of SiO_2 NC nuclei on graphene. The composite has absorption in the range of 200–400 nm but negligible photoluminescence due to the transfer of excited electrons from SiO_2 NCs to rGO. In comparison with isolate and physically mixed amorphous SiO_2 and graphene, the composite has decreased impedance and improved photocurrent under light irradiation, which also shows extraordinarily high activity toward the photocatalytic degradation of organic rhodamine B and 2, 4-dichlorophenol. We believe that the current route presents a new insight into the design and mild synthesis of graphene-based composites with enhanced photo- and photoelectric performance through a mild and simple way.

Author contributions

The manuscript was written through contributions of all authors. All authors have given approval to the final version of the manuscript.

Supplementary data available

EDX pattern of SiO_2 NC/rGO, TEM image of amorphous SiO_2 synthesized without GO, TEM image of physically mixed GO and amorphous SiO_2, TEM images of SiO_2 NC/rGO hybrid prepared with different VTES concentrations, Photographs of GO before and after added into the EtOH–H_2O solution without and with ammonia, Photoluminescence spectrum of SiO_2 NC/rGO excited at 250 nm, TEM image of SiO_2 NC/rGO hybrid prepared with different volume concentrations of ammonia, TEM images of SiO_2 NC/rGO hybrids prepared at different temperatures, Raman spectra of SiO_2 NC/rGO hybrid. The D/G value of rGO increases with the increasing ammonia concentration and reaction temperature, TEM images of SiO_2 NC/rGO hybrid prepared at pure EtOH and water solutions, Photocatalytic degradation curves of RhB and 2, 4-DCP.

Acknowledgements

This work was supported by the National Nature Science Foundation of China (U1407102, 21173077 and 21377038), the National Basic Research Program of China (973 Program, 2013CB632403), the Science and Technology Commission of Shanghai Municipality (14ZR1410700 and 14230710500), the Research Fund for the Doctoral Program of Higher Education (20120074130001) and the Fundamental Research Funds for the Central Universities.

Appendix A. Supplementary data

Supplementary data associated with this article can be found, in the online version, at http://dx.doi.org/10.1016/j.apcatb.2015.06.026

References

[1] J.T. Robinson, S.M. Tabakman, Y. Liang, H. Wang, H.S. Casalongue, D. Vinh, H. Dai, J. Am. Chem. Soc. 133 (2011) 6825–6831.
[2] H. Wang, L. Cui, Y. Yang, H.S. Casalongue, J.T. Robinson, Y. Liang, Y. Cui, H. Dai, J. Am. Chem. Soc. 132 (2010) 13978–13980.
[3] M. Xing, F. Shen, B. Qiu, J. Zhang, Sci. Rep. 4 (2014) 6341.
[4] O.C. Compton, S.T. Nguyen, Small 6 (2010) 711–723.

[5] Y. Zhu, S. Murali, W. Cai, X. Li, J.W. Suk, J.R. Potts, R.S. Ruoff, Adv. Mater. 22 (2010) 3906–3924.
[6] Q. Xiang, J. Yu, J. Phys. Chem. Lett. 4 (2013) 753–759.
[7] H. Wang, H.S. Casalongue, Y. Liang, H. Dai, J. Am. Chem. Soc. 132 (2010) 7472–7477.
[8] Y. Liang, H. Wang, J. Zhou, Y. Li, J. Wang, T. Regier, H. Dai, J. Am. Chem. Soc. 134 (2012) 3517–3523.
[9] K. Todd, H. Chou, S. Amasha, D. Goldhaber-Gordon, Nano Lett. 9 (2009) 416–421.
[10] K.P. Loh, Q. Bao, G. Eda, M. Chhowalla, Nat. Chem. 2 (2010) 1015–1024.
[11] Q. Bao, K.P. Loh, ACS Nano 6 (2012) 3677–3694.
[12] A. Cao, Z. Liu, S. Chu, M. Wu, Z. Ye, Z. Cai, Y. Chang, S. Wang, Q. Gong, Y. Liu, Adv. Mater. 22 (2010) 103–106.
[13] Q. Xiang, J. Yu, M. Jaroniec, Chem. Soc. Rev. 41 (2012) 782–796.
[14] Y. Liang, Y. Li, H. Wang, H. Dai, J. Am. Chem. Soc. 135 (2013) 2013–2036.
[15] W. Li, F. Wang, S. Feng, J. Wang, Z. Sun, B. Li, Y. Li, J. Yang, A.A. Elzatahry, Y. Xia, D. Zhao, J. Am. Chem. Soc. 135 (2013) 18300–18303.
[16] Q. Li, B. Guo, J. Yu, J. Ran, B. Zhang, H. Yan, J. Gong, J. Am. Chem. Soc. 133 (2011) 10878–10884.
[17] K.K. Manga, S. Wang, M. Jaiswal, Q. Bao, K.P. Loh, Adv. Mater. 22 (2010) 5265–5270.
[18] B. Qiu, M. Xing, J. Zhang, J. Am. Chem. Soc. 136 (2014) 5852–5855.
[19] X. Wang, S.M. Tabakman, H. Dai, J. Am. Chem. Soc. 130 (2008) 8152–8153.
[20] M. Xing, X. Li, J. Zhang, Sci. Rep. 4 (2014) 5493.
[21] Y. Li, H. Wang, L. Xie, Y. Liang, G. Hong, H. Dai, J. Am. Chem. Soc. 133 (2011) 7296–7299.
[22] Q. Xiang, J. Yu, M. Jaroniec, J. Am. Chem. Soc. 134 (2012) 6575–6578.
[23] H. Wang, J.T. Robinson, G. Diankov, H. Dai, J. Am. Chem. Soc. 132 (2010) 3270–3271.
[24] M. Xing, W. Fang, X. Yang, B. Tian, J. Zhang, Chem. Commun. 50 (2014) 6637–6640.
[25] H. Wang, J.T. Robinson, X. Li, H. Dai, J. Am. Chem. Soc. 131 (2009) 9910–9911.
[26] S. Pei, H. Cheng, Carbon 50 (2012) 3210–3228.
[27] W.S. Hummers, R.E. Offeman, J. Am. Chem. Soc. 80 (1958) 1339.
[28] C.Y. Kim, S.H. Kim, R. Navamathavan, C.K. Choi, W.Y. Jeung, Thin Solid Films 516 (2007) 340–344.
[29] H. Xiong, S. Tang, H. Tang, P. Zou, Carbohydr. Polym. 71 (2008) 263–268.
[30] N.B. Lân, T. Michael, Analyst 118 (1993) 463–474.
[31] H. Yang, F. Li, C. Shan, D. Han, Q. Zhang, L. Niu, A. Ivaska, J. Mater. Chem. 19 (2009) 4632–4638.
[32] X. Fan, W. Peng, Y. Li, X. Li, S. Wang, G. Zhang, F. Zhang, Adv. Mater. 20 (2008) 4490–4493.
[33] S.J. Kang, B. Kim, K.S. Kim, Y. Zhao, Z. Chen, G.H. Lee, J. Hone, P. Kim, C. Nuckolls, Adv. Mater. 23 (2011) 3531–3535.
[34] Z. Chen, S. Berciaud, C. Nuckolls, T.F. Heinz, L.E. Brus, ACS Nano 4 (2010) 2964–2968.
[35] L. Zhang, Z. Xi, M. Xing, J. Zhang, Int. J. Hydrogen Energy 38 (2013) 9169–9177.
[36] P. Cheng, Z. Yang, H. Wang, W. Cheng, M. Chen, W. Shangguan, G. Ding, Int. J. Hydrogen Energy 37 (2012) 2224–2230.